Nov 6th, 12:00 AM - 12:00 AM

Experimental Seismic Behavior of the CFS-NEES Building: System-Level Performance of a Full-Scale Two-Story Light Steel Framed Building

Kara D. Peterman

Rob L. Madsen

Benjamin W. Schafer

Follow this and additional works at: https://scholarsmine.mst.edu/isccss

Part of the Structural Engineering Commons

Recommended Citation

Experimental seismic behavior of the CFS-NEES building: system-level performance of a full-scale two-story light steel framed building

Kara D. Peterman[1], Rob L. Madsen[2], Benjamin W. Schafer [3]

Abstract

In the summer of 2013, testing of two full-scale cold-formed steel (CFS) framed buildings under seismic excitations took place at the Structural Engineering and Earthquake Simulation Lab (SEESL) at the University at Buffalo. Utilizing the twin shake tables, the two-story building specimens were subjected to ground motions from the 1994 Northridge earthquake. These experiments were conducted as a part of the CFS-NEES experimental effort in an attempt to advance cold-formed steel earthquake engineering and design. Two buildings were tested: the first, a specimen constructed with only structural components (CFS-framed gravity walls, shear walls, floor and roof diaphragms, with OSB sheathing on shear walls and diaphragms); the second began with an exact replica of the first building, but saw the addition of various non-structural systems such as gravity wall sheathing, full diaphragm sheathing, interior partition walls, and exterior weatherproofing. Prior to these experiments, little experimental data existed on full building system behavior for CFS framing. This paper presents results on full-system behavior, specifically examining: drifts, acceleration amplification, shear wall behavior, base shear, diaphragm flexibility, damping, and period of vibration. Comparison to the North American specification for CFS, and design recommendations are also provided.

Introduction

The goals of the CFS-NEES project are: to improve the performance based seismic design of CFS structures and to create high-throughput computational models for use in engineering practice. The experimental component of the

[1] Graduate Research Assistant, Johns Hopkins University, Baltimore, MD, 21218, USA (kpeterm1@jhu.edu)
[2] Senior Project Engineer, Devco Engineering, Enterprise, OR 97828
[3] Professor, Johns Hopkins University, Baltimore, MD, 21218, USA. (schafer@jhu.edu)

project aims to establish benchmark structural response from full-scale building testing; provide information on the performance of key sub-systems (shear walls, diaphragm, gravity framing, and nonstructural elements); and to establish testing to both calibrate and validate computational models.

The overall CFS-NEES effort is summarized in [1]. CFS-NEES testing of key sub-systems, including the shear walls, is provided in [2,3,4] and CFS-NEES testing of fastener-sheathing components critical in the response are performed in [5,6]. Intensive computational modeling of the CFS-NEES building is detailed in [7,8].

Experimental Setup

The full-scale shake table testing at the University of Buffalo was divided into two phases. In the first phase, Phase 1, the building specimen was constructed with structural components only: CFS skeleton, OSB-sheathed shear walls, and OSB-sheathed floor and roof diaphragms. A photograph of the final Phase 1 specimen is shown in Figure 1 below, and is annotated with terminology adopted in this paper.
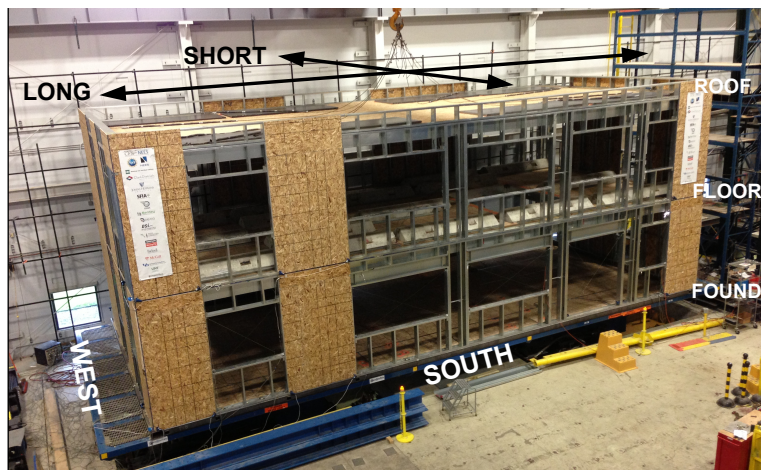

Figure 1: As-built Phase 1 building, annotated with cardinal directions and nomenclature adopted herein: "foundation," "floor," and "roof" for the stories, and "long" and "short" for the axes ("up" is the vertical axis).

Following a large series of non-destructive and destructive testing, this specimen was deconstructed and replaced with the Phase 2 specimen. Ultimately, the

Phase 2 specimen consists of a nominally identical structural system to the Phase 1 building, but is fit-out with nonstructural components. To determine the effect of these components on overall building performance, Phase 2 was divided into five sub-phases, detailed in Figure 2.
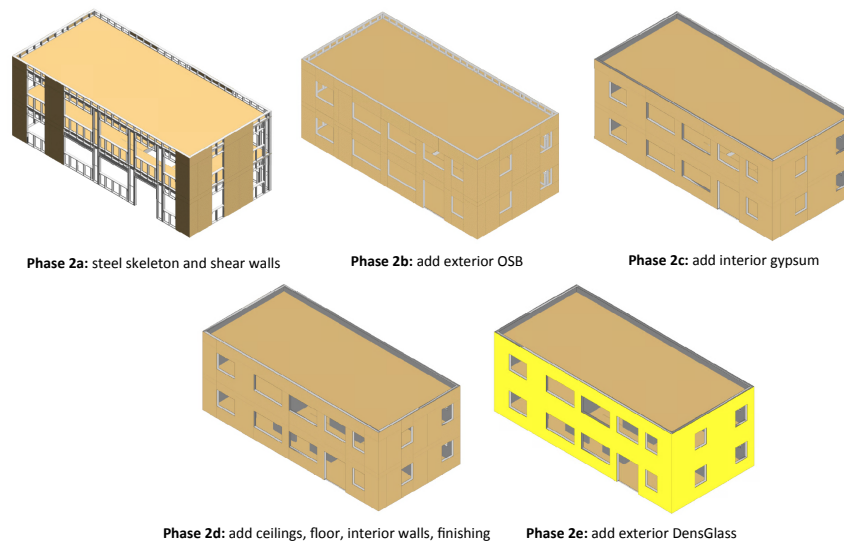

Phase 2a: steel skeleton and shear walls   **Phase 2b:** add exterior OSB   **Phase 2c:** add interior gypsum

Phase 2d: add ceilings, floor, interior walls, finishing   **Phase 2e:** add exterior DensGlass

Figure 2: Illustration of the nonstructural finishing milestones for the Phase 2 specimen

Phase 2a is nominally identical to the Phase 1 building to establish a base-line for comparison. In Phase 2b, OSB is added to the building exterior. Gypsum on the interior face of the exterior walls is added in Phase 2c. Ceilings, partition walls, and staircases are added in Phase 2d. Finally, the building is finished in Phase 2e, with the addition of exterior weatherproofing DensGlass. Non-destructive testing was performed in between these sub-phases.

Two ground motions from the 1994 Northridge earthquake were selected: Canoga Park (PEER NGA0959), and Rinaldi (PEER NGA1063). Based on comparison with the design spectra Canoga Park provides a close approximation to the design basis earthquake (DBE) levels at 100% scale, and Rinaldi provides a close approximation to the maximum considered earthquake (MCE) at 100% scale.

The general test plan for the building specimens involves both white noise and seismic tests. White noise tests excite the specimens at a range of frequencies

and are useful in tracking damage, determining natural frequency, and estimating building stiffness. Table 1 summarizes the test plan for the Phase 1 specimen.

Table 1: Summary of test plan for Phase 1 building. White noise tests are performed in each direction (long, short, up) before and after every seismic level.

ground motion	direction	level
table tuning system ID	3D: long, short, up	0.1 PGA
white noise	long, short, up	0.05 PGA, 0.1 PGA
seismic	1D: long	16% CNP
white noise	long	0.1 PGA
seismic	1D: short	16% CNP
white noise	short	0.1 PGA
seismic	2D: long, short	16% CNP
white noise	long	0.1 PGA
seismic	3D: long, short, up	16% CNP
white noise	long, short, up	0.1 PGA
seismic	3D: long, short, up	44% CNP
white noise	long, short, up	0.1 PGA
seismic	3D: long, short, up	100% CNP
white noise	long, short, up	0.1 PGA

As Table 1 demonstrates, white noise tests were performed before and after every seismic motion, and in the long, short, and up directions. For the Phase 1 and Phase 2a specimens, 16% of full-scale Canoga Park was determined to be nondestructive. Once exterior OSB was added (in Phase 2b) 44% of full-scale Canoga Park was determined to be nondestructive.

System-level results and comparisons

System-level results, including fundamental period, damping, story drift, acceleration amplification, diaphragm flexibility, and base shear are presented below. Comparisons to applicable design codes are presented when relevant.

Fundamental Period

The approximate fundamental period of a given structure is given by ASCE 7-10 §12.8.2.1 Eq. 12.8-7 and, for the CFS-NEES building specimens, the fundamental period (T_n) is determined to be 0.175s. Figure 3 compares the building periods as determined from white noise tests to the code prediction.
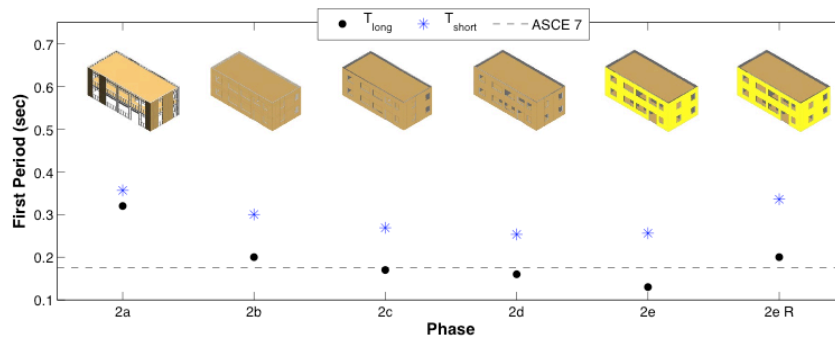
Figure 3: Natural period in the long and short directions, Phase 2a through Phase 2e and Phase 2e tested with the MCE ground motion (2e R). The dashed line represents the ASCE 7-10 prediction.

Experimentally, it is impossible to determine one value of the natural period. Instead, natural period must be determined for both long and short directions of the ground motion since the building is unsymmetric. However, it is evident from Figure 3 that both T_{long} and T_{short} for the structural system (Phase 1) are quite far from the code predictions but approach the $T_n = 0.175s$ prediction as nonstructural elements are added.

Inherent structural damping

FEMA P-750, the National Earthquake Hazards Reduction Program (NEHRP) Recommended Provisions (2009) states, in its Modifications to Chapter 18 [of ASCE 7-10], Seismic Design Requirements for Structures with Damping Systems that inherent structural damping (ζ) shall be assumed to be ≤5% unless testing motivates use of a larger value. Early CFS-NEES modeling assumptions assumed $\zeta = 5\%$ so it is to this initial benchmark comparisons are made, as shown in Figure 4 below.
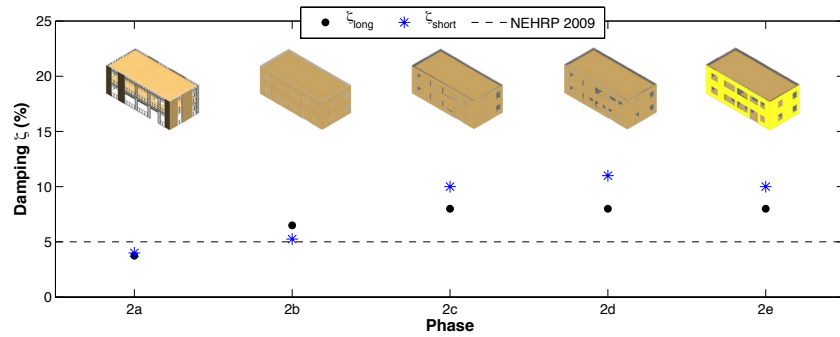
Figure 4: Comparison of percent damping from experimental white noise tests to NEHRP recommendation in FEMA P-750. Error: +/- 1%

Figure 4 demonstrates the percent damping as determined from pre-damage white noise tests. Only the Phase 2a (Phase 1 also has an identical percent as Phase 2a) percent damping are below the NEHRP/FEMA P-750 recommended value of 5%. Damping drastically increases once the specimens are finished with exterior OSB sheathing and gypsum on the inside of the exterior walls. In Phases 2d and 2e, however, damping remains relatively constant at 10% in the short direction and 8% in the long direction.

Acceleration amplification

Acceleration amplification is determined by taking the ratio of an accelerometer at the floor or roof levels to the foundation acceleration. In this manner, an amplification factor may be determined, and demonstrates how the buildings experience accelerations through the total height. Amplification factors for selected seismic tests for the long, short and up directions are shown in Table 2.

Table 2: Corner acceleration amplification and foundation average acceleration at peak drift for selected seismic tests in three directions

Test	Ground Motion	LONG			SHORT			UP		
		Found*	Floor	Roof	Found*	Floor	Roof	Found*	Floor	Roof
P1S05	CNP 44%	0.21	2.07	3.42	0.21	2.35	2.44	0.31	-	1.11
P2bS05	CNP 44%	0.24	1.46	1.71	0.21	1.66	1.86	0.27	-	1.13
P2cS05	CNP 44%	0.23	1.56	1.79	0.19	1.38	1.92	0.26	-	1.19
P2dS05	CNP 44%	0.24	1.42	1.73	0.18	1.29	2.09	0.3	-	1.12
P2eS05	CNP 44%	0.26	1.24	1.52	0.21	1.14	1.88	0.27	-	1.33
P1S07	CNP 100%	0.61	2.52	3.30	0.48	1.92	2.51	0.68	-	1.35
P2eS07	CNP 100%	0.61	1.48	1.73	0.52	1.17	1.94	0.59	-	1.38
P2eS09	RRS 100%	1.13	1.64	1.82	0.82	1.32	1.34	1.27	-	1.18

*Average acceleration across foundation-level accelerometers. Units are g

The Phase 1 specimen experiences significant amplification in the long and short directions, as shown in the P1S05 and P1S07 tests. Phases 2b through 2d experience similar amplifications, and all are relatively small compared to the Phase 1 building. Amplification decreases again in Phase 2e, indicating that the nonstructural components with the greatest acceleration effect are exterior OSB (Phase 2b) and exterior DensGlass (Phase 2e).

Story drift

Interstory drift is show for the long and short directions and for both first and second stories for the Phase 1 DBE motion in Figure 5 below.
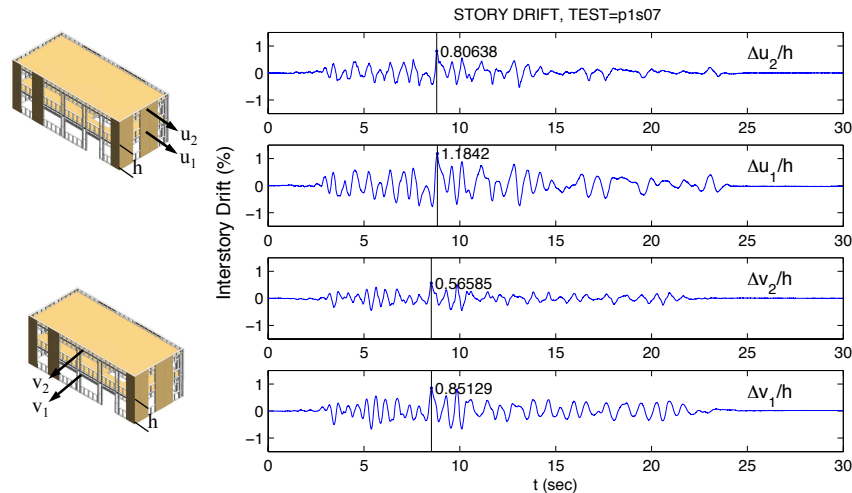

Figure 5: Story drift in the long and short directions for the Phase 1 DBE test (100% CNP)

Peak drift occurred in the first story in the long direction, and is approximately 1.2%. This value is well-below expectations from shear wall tests [2,3,4], which, for shear walls framed similarly to those in the test buildings, produced drifts of approximately 4%. Drift across construction phases is summarized in Table 3.

Table 3: Summary of interstory drift across selected seismic levels, in the long and short directions for both first and second stories.

		MAX % STORY DRIFT (Δ/h)			
		LONG		SHORT	
Test Name	Ground Motion	$\Delta u_1/h$	$\Delta u_2/h$	$\Delta v_1/h$	$\Delta v_2/h$
-	-	%	%	%	%
P1S05	CNP 44%	0.55	0.38	0.36	0.29
P2bS05	CNP 44%	0.19	0.29	0.11	0.21
P2cS05	CNP 44%	0.12	-0.22	0.11	0.17
P2dS05	CNP 44%	0.11	-0.19	0.08	-0.15
P2eS05	CNP 44%	0.08	-0.20	0.06	-0.14
P1S07	CNP 100%	1.18	0.81	0.85	0.56
P2eS07	CNP 100%	0.25	-0.48	0.16	-0.32
P2eS09	RRS 100%	0.67	-0.72	0.45	0.49

As the building is finished with nonstructural elements, total drift decreases, with the largest decreases occurring with the addition of exterior OSB sheathing (Phase 2b). The maximum drift experienced for the MCE is in the short direction, indicating a change in the directionality of the building strength. Furthermore, drift for the MCE is reduced to 0.72% with no residual drift observed post-test.

Diaphragm flexibility

The ASCE 7-10 definition of diaphragm flexibility may be summarized as follows: if the maximum diaphragm deflection is greater than twice the average drift of a vertical element, the diaphragm is flexible. These values for test P1S07 are presented in Figure 6. Note that ASCE 7-10 presumes this comparison is based on static analysis, but it is presented here for dynamic analysis.
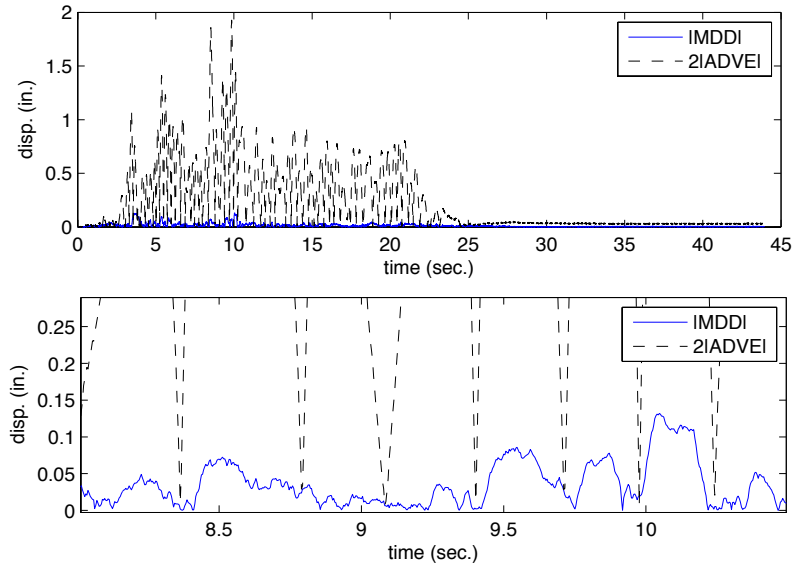
Figure 6: At top, maximum diaphragm deflection compared to twice the average drift of a vertical element for excitation 100% CNP in 3D. Bottom plot magnifies maximum diaphragm deflection near the peaks in the Canoga Park ground motion

Because the maximum diaphragm deflection is so small in comparison to the building drift, the diaphragm may be presumed to be rigid, despite that ASCE 7-10 §12.3.1.1 states that for the building design, the diaphragm may be idealized as flexible. However, it is clear from Figure 6 that this measure of flexibility is incomplete. To further explore diaphragm flexibility, diaphragm twist and shear are shown in Figure 7 for the Phase 1 100% Canoga Park test. The structural system-only tests demonstrated the largest rotation and shear angles of all of the tests, and are thus presented herein.
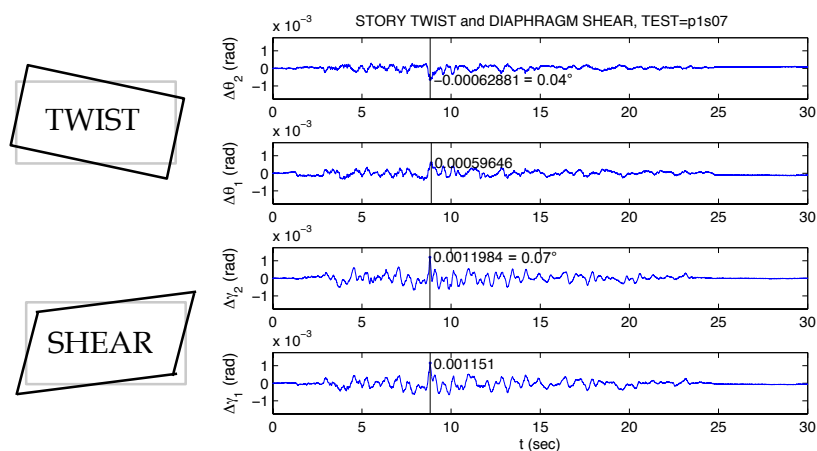
Figure 7: Story twist and diaphragm shear for Phase 1, excitation 100% Canoga Park in 3D

While 0.04 degrees of twist and 0.07 degrees of shear are non-zero, they are small. To understand the impact, consider the effect of the rotations on the drift at a wall line. Wall line drift is comprised of translation, rotation, and shear—if wall lines experience these components unequally, the building displaces torsionally. From these results, it is evident that the simplified ASCE 7 definition of diaphragm flexibility may not capture the complex diaphragm behavior observed. The shortcomings of this definition are clear. Without a means of assessing degree of rigidity or flexibility, the comparison between diaphragm deflections and vertical drift is insufficient.

Isolated ("Type I") versus interacting ("Type II") shear walls

By installing load cells in the hold down anchor bolts, it is possible to approximate the distribution of shear wall anchor forces at a given moment in time. When the wall is in tension, the anchor bolt compresses the load cell. Because the load cells can only read compression on the load cell, they can only measure when the hold downs are in tension. Figure 8 shows the distribution of hold down force as measured from the load cells for four tests: P1S07, P2aS04, P2bS05, and P2eS09. The downward (red) bars indicate that the shear wall hold down and chord stud is in tension, while the upward (blue) bars indicate that the hold down and chord stud is in the compression. Since the load cells are unable to accurately gauge magnitude when the hold down is in compression, the upward (blue) bars only indicate direction, not magnitude.
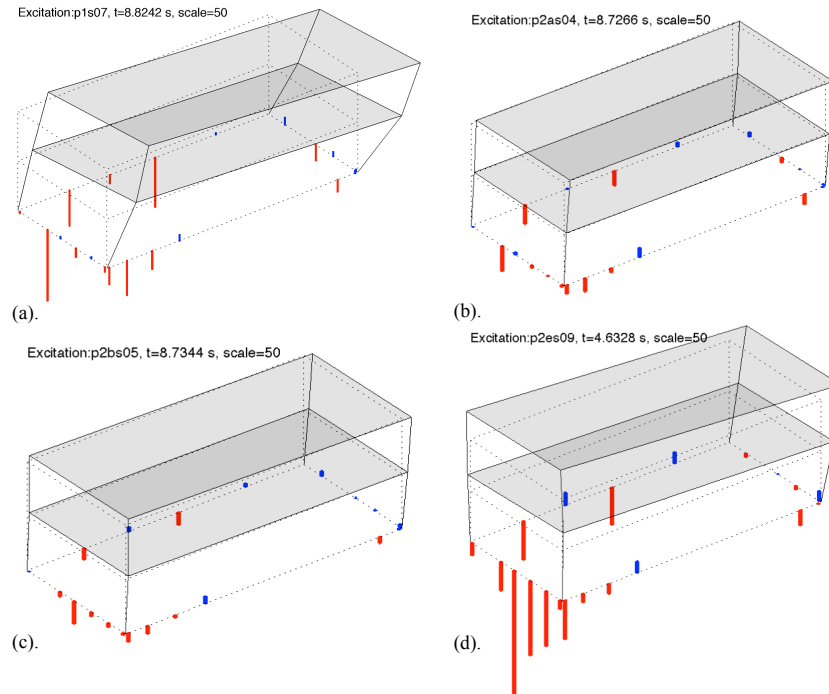
Figure 8: Distribution of load in shear wall hold downs at peak story drift for (a) test P1S07 (100% CNP, in 3D) (b). test P2aS04 (16% CNP in 3D) (c). test P2bS05 (44% CNP in 3D) and (d). test P2eS09 (100% RRS in 3D)

Figure 8(a) illustrates both Type I and Type II shear wall behavior: on the west wall, the shear walls clearly exhibit classical Type I behavior (tension and compression pairs at each chear wall) while on the south wall, both Type I and Type II (southwest shear walls) behaviors are observed. The north wall similarly exhibits both behaviors. At lower excitation levels, the building specimen performs commensurately: Figure 8(b) depicts load distributions much like those experienced in the Phase 1 testing. From this comparison it evident that excitation magnitude does not unduly influence shear wall behavior/force distribution. Once exterior OSB sheathing is added to the building specimen (Phase 2b) Type II behavior becomes more prominent in the south, west, and east walls (Figure 8(c)). The finished building specimen (Phase 2e, Figure 8(d)), however, demonstrates more unique behavior, with much of the west side of the building in compression. Despite this, the north wall exhibits classical Type I behavior, as it typically assumed in design.

Shear wall chord stud strength

For the Phase 1 specimen, an error in construction drawings lead to a back-to-back first story chord stud terminating early such that only a single stud framed into the second story. This error effectively reduced the overstrength factor (ASCE 7, 2010) from Ω_o = 3.0 to Ω_o = 1.5 for that chord stud. During the Phase 1 design basis earthquake test (100% Canoga Park in 3D), this chord stud yielded and ultimately buckling locally in the flange. The buckling of the stud indicates that the forces experienced by the studs are greater that what would be predicted using the elastic base shear divided by the current inelastic response modification factor, R = 6.5 (ASCE 7, 2010). Once this error was remedied in the Phase 2 building, the chord stud behaved elastically for the remainder of testing. Thus, it is clear that Ω_o = 1.5 would not be sufficient and that Ω_o = 3.0 should be continued.

Estimation of base shear

As previously mentioned, base shear per shear wall may be estimated from shear wall hold down force readings. Given a shear wall width w, height h, and hold down forces F, base shear V may be determined from the force couple V*h = F*w. Figure 9(a) details this assumption:
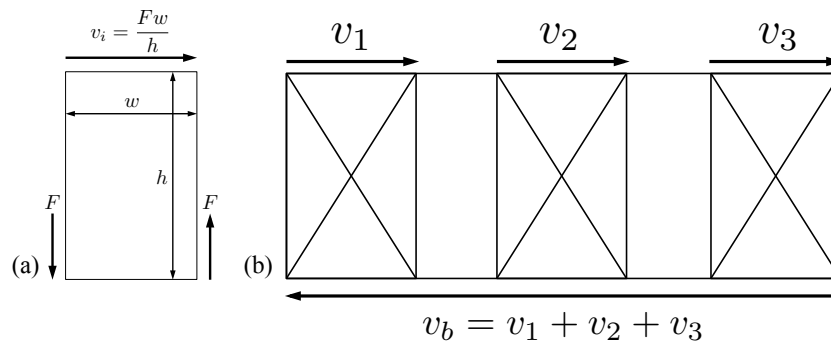

Figure 9: (a). Force couple assumption for determining base shear per foot (b) wall line base shear per foot as the superposition of the individual shear wall base shears per foot

Across a wall line, shear wall base shear V may be superimposed across the wall line. For a hypothetical wall line, this results in the following assumption: that total wall line base shear is a result of the superposition of individual shear wall base shears (per foot). This concept is illustrated in Figure 9(b).

From these simple assumptions, base shear distribution across the wall line may be determined, as shown in Table 4. Peak base shear forces are experienced during the DBE ground motion, P1S07. As the load cells installed in the hold downs cannot accurately record wall compression, positive values should be noted for their direction only (wall compression) and not their magnitude.

Table 4: Base shear at peak drift for wall lines

		v_b @ δ_{max}			
	Ground Motion	**SOUTH**	**WEST**	**NORTH**	**EAST**
	-	*kip/ft*	*kip/ft*	*kip/ft*	*kip/ft*
p1s05	CNP 44%	-1.23	-4.15	-5.43	-1.28
p2bs05	CNP 44%	-0.78	-1.42	-3.01	-0.86
p2cs05	CNP 44%	0.40	0.62	0.31	1.43
p2ds05	CNP 44%	0.59	0.59	1.29	1.59
p2es05	CNP 44%	0.96	1.35	2.00	1.75
p1s07	CNP 100%	-2.40	-6.97	-9.83	-2.15
p2es07	CNP 100%	0.41	0.21	1.09	2.00
p2es09	RRS 100%	-1.02	-3.44	-2.42	1.65

Because peak base shear is often experienced prior to peak drift, maximum base shear is presented in Table 5.

Table 5: Maximum base shear for wall lines

		max v_b			
	Ground Motion	**SOUTH**	**WEST**	**NORTH**	**EAST**
	-	*kip/ft*	*kip/ft*	*kip/ft*	*kip/ft*
p1s05	CNP 44%	-1.76	-4.60	-6.42	-4.88
p2bs05	CNP 44%	-1.09	-2.14	-3.76	-2.15
p2cs05	CNP 44%	-0.23	-0.10	-0.41	-0.46
p2ds05	CNP 44%	-0.05	0.36	0.32	0.35
p2es05	CNP 44%	0.39	0.58	1.53	1.31
p1s07	CNP 100%	-3.29	-8.76	-11.48	-8.63
p2es07	CNP 100%	-0.76	-2.31	-0.54	-1.24
p2es09	RRS 100%	-1.06	-4.80	-2.67	-2.91

A setback in comparing experimental base shear to design code provisions is that experimental data is unable to provide a single foundation base shear value, instead providing base shear in the long and short directions. ASCE 7-10 provides a formulation for base shear based on total seismic weight and the base shear coefficient, which results in $V_b = 11$ kips.

From Table 4 above, V_b in the long direction estimate $V_b = 12$ to 13 kips at peak drift based on experimental data for test P1S07. The short direction base shear is greatly reduced at peak drift, and is approximately 8 to 9 kips. Regardless of the present inability to combine the long and short direction base shears, the

experimental values are within those predicted by ASCE 7-10. Shear walls in the Phase 1 structure carry reasonably large base shears but once finishing nonstructural elements are added, the lateral force is carried by other systems. This progression can be seen in the difference between the P1S05 and P2eS05 wall line base shear values. Despite the simplicity of the ASCE 7 base shear equation, the current recommendation is that it is adequate for use in design though further calibration is necessary to form a definitive conclusion.

Conclusions

System-level building response is presented for the CFS-NEES full-scale experimental work. Performance of key sub-systems like the floor diaphgram, shear walls, and nonstructural systems are also presented. Comparisons to applicable design codes are also detailed. The building responds as a system, not as a superposition of sub-systems. Furthermore, the nonstructural systems significantly contribute to full-system behavior. The specimens behavior suggest discrepancy from the design codes yet provide motivation for future improvement.

Acknowledgments

References

[1] Schafer BW, Ayhan D, Leng J, Liu P, Padilla-Lllano D, Peterman KD, Stehman M, Buonopane SG, Eatherton M, Madsen R, Manley B, Moen CD, Nakata N, Rogers C, Yu C. The CFS-NEES effort: Advancing Cold-Formed Steel Earthquake Engineering. Proceedings of the 10th National Conference in Earthquake Engineering, Earthquake Engineering Research Institute, Anchorage, AK, 2014.

[2] P. Liu, K.D. Peterman, B.W. Schafer (2012). "Test Report on Cold-Formed Steel Shear Walls" Research Report, CFS-NEES, RR03, June 2012, access at www.ce.jhu.edu/cfsnees

[3] P. Liu, K.D. Peterman, C. Yu, B.W. Schafer (2012) "Cold-formed steel shear walls in ledger-framed buildings", Annual Stability Conference, Structural Stabilitiy Research Council, April 2012, Grapevine, Texas.

[4] Liu, P., Peterman, K.D., Yu, C., Schafer, B.W. (2012a). "Characterization of cold-formed steel shear wall behavior under cyclic loading for the CFS-NEES building." Proc. of the 21st Int'l. Spec. Conf. on Cold-Formed Steel Structures, 24-25 October 2012, St. Louis, MO, 703-722.

[5] K.D. Peterman, B.W. Schafer (2013). "Hysteretic shear response of fasteners connecting sheathing to cold-formed steel studs" Research Report, CFS-NEES, RR04, January 2013, access at www.ce.jhu.edu/cfsnees

[6] K.D. Peterman, N. Nakata, B.W. Schafer (2012) "Cyclic Behavior of Cold-Formed Steel Stud-to-Sheathing Connections" 15th World Conference on Earthquake Engineering, September 24-28, Lisbon, Portugal.

[7] Leng, J., Schafer, B.W., Buonopane, S.G. (2013). "Modeling the seismic response of cold-formed steel framed buildings: model development for the CFS-NEES building." Proceedings of the Annual Stability Conference - Structural Stability Research Council, St. Louis, Missouri, April 16-20, 2013, 17pp.

[8] Leng, J., Schafer, B.W., Buonopane, S.G. (2012). "Seismic Computational Analysis of CFS-NEES Building." Proc. of the 21st Int'l. Spec. Conf. on Cold-Formed Steel Structures, 24-25 October 2012, St. Louis, MO, 801-820.

[9] R.L. Madsen, N. Nakata, B.W. Schafer (2011) "CFS-NEES Building Structural Design Narrative", Research Report, RR01, access at www.ce.jhu.edu/cfsness, October 2011, revised RR01b April 2012, revised RR01c May 2012.

[10] N. Nakata, B.W. Schafer, and R.L. Madsen (2012) "Seismic Design of Multi-Story Cold-Formed Steel Buildings: the CFS-NEES Archetype Building," 2012 Structures Congress, March 2012, Chicago, Illinois. 1507-1517.

[11] ASCE 7-05: ASCE Standard [ASCE/SEI 7-05] "Minimum Design Loads for Buildings and Other Structures." 2005 edition. American Society of Civil Engineers

[12] AISI S213-07: AISI Standard "North American Standard for Cold-Formed Steel Farming –Lateral Design", 2007 edition. American Iron and Steel Institute

[13] AISI-S100. (2007). North American Specification for the Design of Cold-Formed Steel Structural Members, American Iron and Steel Institute, Washington, D.C.

[14] SSMA. (2001). *Product Technical Information, ICBO ER-4943P*, Steel Stud Manufacturers Association, <www.ssma.com>.